TA0343
Technical article

Everything about STMicroelectronics' 3-axis digital MEMS gyroscopes

Executive summary

STMicroelectronics (ST), the leading worldwide supplier of MEMS motion sensors[a], introduced in early 2010 an innovative 3-axis digital gyroscope in a 4 x 4 x 1.1 mm LGA package. Its innovative "beating heart" architecture, leveraging a single driving mass design for pitch, roll and yaw axes, coupled with ST's consolidated MEMS manufacturing expertise, pioneered the way for this gyroscope to become widely adopted and successfully implemented in best-selling smartphones and other handheld device platforms, generating excellent market feedback.

The following facts are testimony to the success of this device:

- ST has shipped more than 1.4 billion MEMS sensors to date and its dedicated 8-inch MEMS fabrication line, which was among the first in the world, currently produces more than 3 million devices a day.
- ST's gyroscopes have been adopted in many smartphone applications and other consumer electronics by a large number of customers. This unique, wide-spread use has allowed ST to rapidly gain customer appreciation and feedback and accelerate the trajectory of gyroscope sensor development.
- ST's in-house MEMS manufacturing expertise ensures the quality and performance of each MEMS gyroscope. ST has been able to do in-house stack assembly for MEMS die and ASIC die in a single LGA 4 x 4 x 1.1 mm package since 2005.
- ST's "beating heart" single driving structure allows perfect control of the single driving frequency at which the movable mass is oscillating. Other solutions on the market, presenting different driving masses to implement multi-axis capability, lead to spurious noise coupling from one axis to the other, irremediably degrading gyroscope performance. ST's innovative approach allows gyroscopes to provide very high resolution and stability, suitable for gaming and navigation applications.
- Other suppliers use complex assembly techniques for piezoelectric gyroscopes, while ST's single MEMS driving structure and unrivalled MEMS manufacturing expertise simplify the assembly procedure while producing excellent performance in terms of zero-rate level and sensitivity stability over temperature and time.
- The embedded self-test in ST's 3-axis digital gyroscope is an additional key feature that allows the gyroscope to be tested during final product assembly without requiring physical device movement.

a. Source iSuppli, Dec 2010.

Contents

List of figures

1 Introduction

STMicroelectronics' innovative, reliable and cost-effective MEMS sensors have revolutionized the way people interact with everyday technology, making it easier and more user-friendly. The MEMS sensors family ranges from 2- and 3-axis linear accelerometers to single- and multi-axis gyroscopes, and sensor modules. Encompassing the entire supply chain, ST brings its customers a competitive advantage with complete, reliable and cost-effective solutions, ensuring prompt time-to-volume and time-to-market to effectively address high-volume applications in consumer and industrial market segments.

Thanks to its manufacturing expertise in MEMS, ST is the sole sensor supplier in the world who has delivered more than 1.4 billion sensors to a worldwide customer base and is capable of high-volume production to meet the market's demands. ST’s manufacturing expertise also guarantees high performance and product reliability. Every MEMS sensor is factory tested and trimmed so that for most consumer applications, no additional sensor calibrations are required. With a built-in self-test feature, the end user can quickly verify the sensor’s operation without physically tilting or rotating the sensor which allows accelerating time-to-market for mass production.

The purpose of this technical article is to provide a clear picture of the performance of ST's L3G4200D 3-axis MEMS digital gyroscope and guidelines for its use in consumer and industrial applications.
Section 2: The beauty of the MEMS single driving structure design shows the elegant design of the MEMS single driving structure.
Section 3: Excellent performance of key parameters describes the excellent performance of key parameters and their characterization data.
Section 4: Comparing ST’s gyroscopes to the competition focuses on the comparison between ST’s gyroscope and a gyroscope currently on the market.
Section 5: Getting started with ST’s 3-axis digital gyroscope gives practical guidelines for designing the gyroscope in applications and how to convert raw data into angular velocity and angular displacement.
Section 6: Gyroscope-enabled gaming and navigation shows how to integrate the gyroscope into a handheld device for gaming and navigation applications.

2 The beauty of the MEMS single driving structure design

ST's 3-axis digital gyroscopes use an innovative, single driving structure design (beating heart) as shown in *Figure 1*. This unique, single driving structure design in the current market has only one driving mass for the measurement of the angular rate of all three axes, based on the Coriolis principle. *Figure 2* and *Figure 3* show the die of the MEMS structure and ASIC, respectively.

Figure 1. Single driving structure of 3-axis digital gyroscopes

Figure 2. MEMS structure die of 3-axis digital gyroscopes

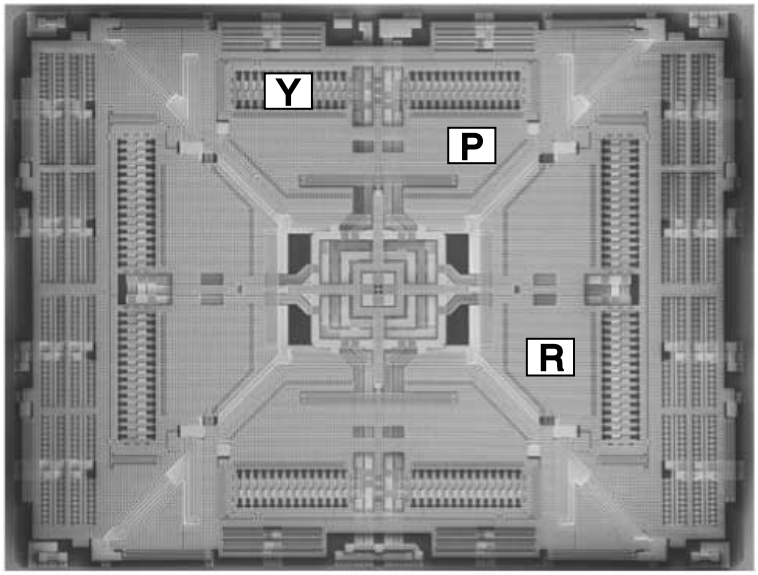

Figure 3. ASIC die of 3-axis digital gyroscopes

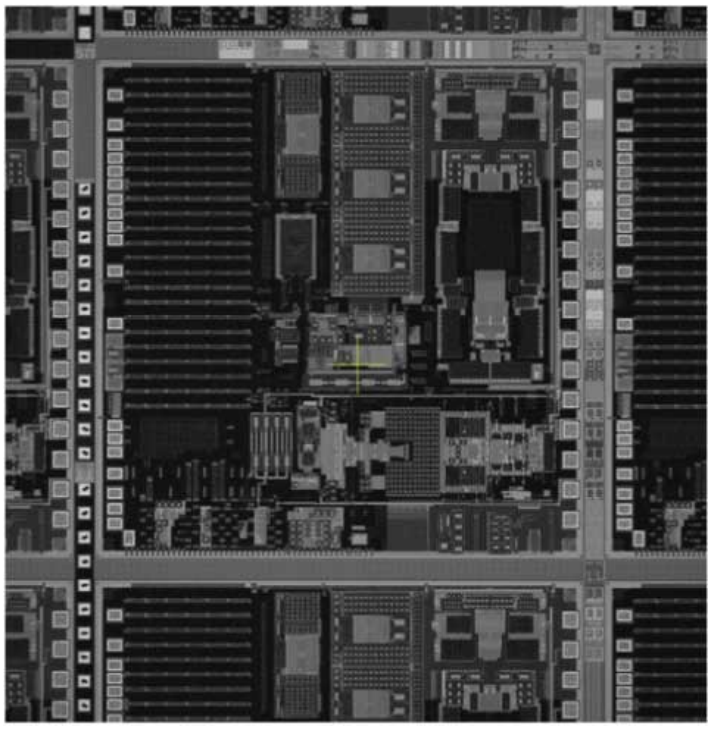

Figure 4. Demonstration of single driving mass

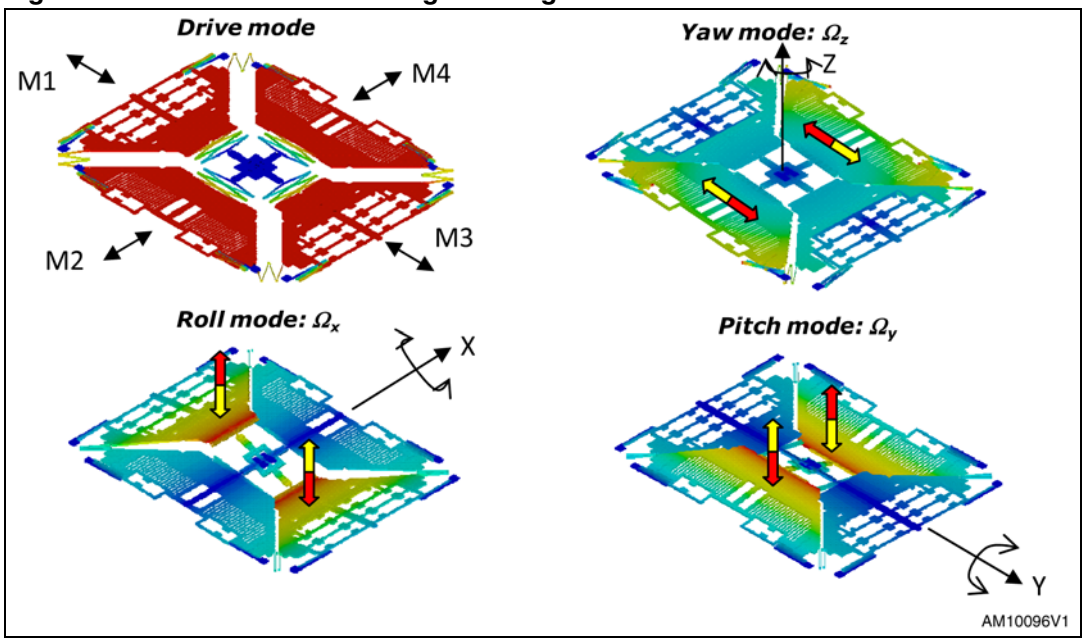

Figure 4 shows how the beating heart structure works.

Definitions

- Roll axis is defined as the Y-axis. Angular rotation along the Y-axis Ω_y is called pitch mode which will cause the pitch angle to change
- Pitch axis is defined as the X-axis. Angular rotation along the X-axis Ω_x is called roll mode which will cause the roll angle to change
- Yaw axis is defined as the Z-axis. Angular rotation along the Z-axis Ω_z is called yaw mode which will cause the yaw angle to change

In *Figure 2*, Y, P and R stand for the sensing masses for yaw, pitch and roll modes. The perfect symmetry and the differential approach adopted in the structure design assure a high level of rejection to linear acceleration acting on the sensor (i.e. vibration). The driving mass shown in *Figure 4* consists of 4 parts M1, M2, M3 and M4. They move inward and outward simultaneously at a certain frequency in the horizontal plane. When an angular rate is applied on the Z-axis, due to the Coriolis effect, M2 and M4 will move in the same horizontal plane in opposite directions as shown by the red and yellow arrows. When an angular rate is applied on the X-axis, then M1 and M3 will move up and down out of the plane due to the Coriolis effect. When an angular rate is applied to the Y-axis, then M2 and M4 will move up and down out of the plane.

Whenever the Coriolis effect is detected, the continuous movement of the driving mass will cause a capacitance change ΔC which is picked up by the sensing structure and then ΔC is converted to a voltage signal by the internal circuitry [1]. The voltage signal, which is proportional to the applied angular rate, is then converted to 16-bit digital format and stored in the internal data registers. External microprocessors can retrieve gyroscope measurements by accessing these data registers through the I^2C or SPI interfaces.

When linear acceleration is applied along the X-, Y- or Z-axis, thanks to the differential approach adopted, the driving masses (M1 and M3 or M2 and M4) will move in the same direction which will cause ΔC to be 0. This means that the gyroscope is able to reject linear acceleration such as shock or vibration.

Other 3-axis MEMS gyroscopes on the market use either three single driving structures or one single, plus one dual driving structure, in some cases even resonating at different frequencies. The natural mismatch between driving frequencies, even when designed to be the same, will cause spurious noise on gyroscope output signals. The high level of symmetry used by ST in the design and manufacturing of driving and sensing structures doesn't present this issue, allowing ST's gyroscopes to further reduce noise and improve robustness.

3 Excellent performance of key parameters

The terms used in this technical article are defined as follows:

Power supply (V): This parameter defines the operating DC power supply voltage range of the MEMS gyroscope. It is recommended to keep Vdd clean with minimum ripple. A good practice is to use an ultra-low noise, low-dropout regulator to power the MEMS gyroscope.

Power supply current (mA): This parameter defines the typical current consumption when the MEMS gyroscope is operating in normal mode.

Power supply current in sleep mode (mA): This parameter defines the current consumption when the MEMS gyroscope is in sleep mode. To reduce power consumption and have a faster turn-on time, in sleep mode the driving circuitry is on, the mechanical mass is kept oscillating and the reading chain is turned off. For analog gyroscopes, an external pin can be used to configure this mode. For digital gyroscopes, users can configure a control register through the I^2C/SPI interface for this mode. Other suppliers don't provide a sleep mode (or standby mode).

Power supply current in power-down mode (µA): This parameter defines the current consumption when the MEMS gyroscope is powered down. During this mode, both the mechanical sensing structure and reading chain are turned off. For analog gyroscopes, an external pin can be used to configure this mode. For digital gyroscopes, users can configure the control register through the I^2C/SPI interface for this mode. Full access to the control registers through the I^2C/SPI interface is guaranteed also in power-down mode.

Full-scale range (dps): This parameter defines the measurement range of the gyroscope in degrees per second (dps). When the applied angular velocity is beyond the full-scale range, the gyroscope output signal will be saturated. However, this saturation will not damage the gyroscope and will have no negative impact on its performance.

Zero-rate level (V or LSBs): This parameter defines the zero-rate level voltage for analog gyroscopes when no angular velocity is applied to the MEMS gyroscope sensing axis. It is not ratiometric to the power supply voltage and ideally it is equal to the output reference voltage Vref on a dedicated output pin for analog gyroscopes. For digital gyroscopes, the zero-rate level is typically 0 LSBs. It is also not ratiometric to the power supply voltage.

Sensitivity (mV/dps or mdps/LSB): Sensitivity in mV/dps defines the relationship between 1 dps and the analog gyroscope's output voltage change over the zero-rate level. Using this parameter the user can convert the gyroscope’s output voltage signal into angular velocity. For digital gyroscopes, sensitivity (mdps/LSB) is the relationship between 1 LSB and milli dps. So the user can directly convert a digital gyroscope’s measurement in LSBs to angular velocity.

Sensitivity change vs. temperature (%/°C): This parameter defines the sensitivity change in percentage per °C when the temperature varies from 25°C room temperature for analog gyroscopes. For digital gyroscopes, it defines the sensitivity change in percentage (%) over the operating temperature range specified in the datasheet (for example, from -40°C to +85°C).

Zero-rate level change vs. temperature (dps/°C): This parameter defines the change in the zero-rate level per °C when the temperature varies from 25°C for analog gyroscopes. For digital gyroscopes, it defines the zero-rate level change in dps/°C over the operating temperature range.

Non-linearity (% FS): This parameter defines the maximum error between the gyroscope's outputs and the best-fit straight line in percentage with respect to the full-scale (FS) range.

System bandwidth (Hz): This parameter defines the frequency of the angular velocity signal from DC to the built-in bandwidth (BW) that the gyroscopes can measure. If the user's application requires narrower bandwidth, then an external RC low-pass filter can be applied on the output pin of the analog gyroscopes. For digital gyroscopes, a dedicated register can be modified to adjust the gyroscope's bandwidth.

Rate noise density (dps/√ Hz): This parameter defines the standard resolution for both analog and digital gyroscopes that users can get from the gyroscopes' outputs together with the BW parameter. A higher BW leads to a higher noise level or lower resolution. This parameter is also equivalent to an angular random walk in degree/√hour.

Self-test (mV or dps): For analog gyroscopes, there is a dedicated input pin to enable the self-test. For digital gyroscopes, there are two dedicated bits in a control register to enable the self-test. This feature can be used to verify if the gyroscope is working properly or in order to not physically rotate the gyroscope after it is assembled on a PCB. When the self-test is enabled, an internal electrostatic force is generated to move the masses to simulate the Coriolis effect. If the gyroscope's outputs are within the specified self-test values in the datasheet, then the gyroscope is working properly. Therefore, the self-test feature is an important consideration in a user's end-product mass production line. Other suppliers don't have this self-test feature.

The primary key parameters used to judge the performance of a 3-axis MEMS digital gyroscope are the following:

- Noise density level (dps/√Hz)
- Non-linearity (% of FS)
- Zero-rate level change vs. temperature (dps/°C)
- Sensitivity change vs. temperature (%/°C)
- Zero-rate level distribution, part by part
- Sensitivity distribution, part by part

3.1 Noise density level

The noise density level (dps/√Hz) can be retrieved from an Allan Variance plot. The Allan Variance (AVAR), developed by Dr. David Allan, is a method of analyzing a time series to determine the system noise level as a function of the averaging time. Traditionally, it has been used to analyze the stability of clocks, but we can use it to measure gyroscope noise density. The Allan Variance is defined as given in *Equation 1:*

Equation 1

$$\sigma_y^2(\tau,N) = \mathrm{AVAR}(\tau,N) = \frac{1}{2\tau^2(N-2)}\sum_{i=0}^{N-3}\left(x_{i+2} - 2x_{i+1} + x_i\right)^2$$

where,

- N is the number of samples of the time series
- τ is the averaging time in seconds
- x is the gyroscope output measurement time series

The Allan Variance plot of a 3-axis MEMS digital gyroscope is shown in *Figure 5*.

Figure 5. Allan Variance plot of a 3-axis digital gyroscope

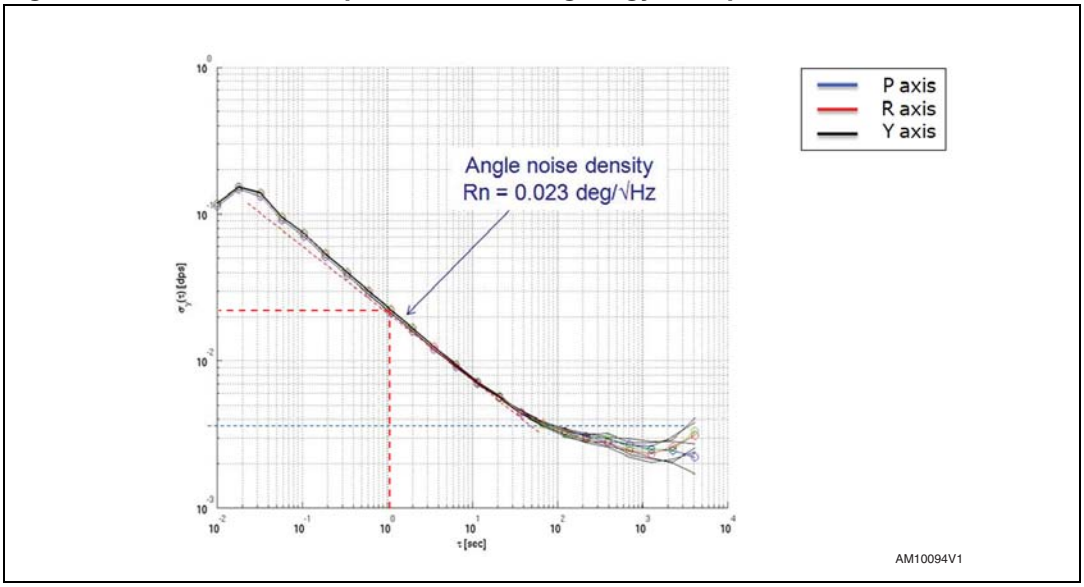

In *Figure 5*, at 1 second, the square-root of the Allan Variance value is about 0.023 dps. So the noise density level is 0.023 dps/√Hz 1-sigma based on the assumption that the gyroscope noise is white. Multiplying this value by 60, the angular random walk (ARW) will be 1.38 degree/√Hour. This means that after 1 hour, the angular uncertainty will be 1.38 degrees.

Table 1 shows the characterization data for the noise density based on 6 DUTs (device under test), measured at each full-scale range (250, 500, 2000 dps) with an ODR of 200 Hz and a BW of 12.5 Hz. The average noise density is 0.029 dps/√Hz which shows that the gyroscope has very low noise density level.

Table 1. Noise density characterization data(1)

DUT	FS	RnP	RnR	RnY
[#]	[dps]	[dps/√HZ]		
1	250	0.028	0.030	0.028
	500	0.025	0.024	0.025
	2000	0.025	0.024	0.025
2	250	0.040	0.036	0.030
	500	0.026	0.026	0.023
	2000	0.035	0.024	0.025
3	250	0.022	0.036	0.030
	500	0.024	0.033	0.026
	2000	0.024	0.030	0.025
4	250	0.044	0.040	0.026
	500	0.030	0.028	0.027
	2000	0.027	0.025	0.024
5	250	0.035	0.029	0.032
	500	0.031	0.028	0.029
	2000	0.029	0.028	0.029
6	250	0.033	0.028	0.031
	500	0.026	0.029	0.030
	2000	0.028	0.027	0.029

1. Average noise density measured of 0.029 dps / √Hz

3.2 Non-linearity

Ideally, the gyroscope's output should be proportional to the input angular velocity. Non-linearity is defined as the maximum deviation between the gyroscope's output and the input angular rate from the best-fit straight line over the full-scale range.

Figure 6 shows the characterization data of non-linearity at different full-scale ranges. The non-linearity for a 250 dps and 500 dps full-scale range is below 0.2% FS. For example, at a 250 dps FS range, the non-linearity for the X-axis is 0.11% of FS = 0.11% * 250 dps = 0.275 dps. This value is negligible so the effect on the overall performance for common consumer applications can be ignored.

Figure 6. Non-linearity characterization data

	NLP	NLR	NLY
FS	[%FS]	[%FS]	[%FS]
250	0.11	0.09	0.10
500	0.15	0.16	0.14
2000	0.28	0.30	0.32

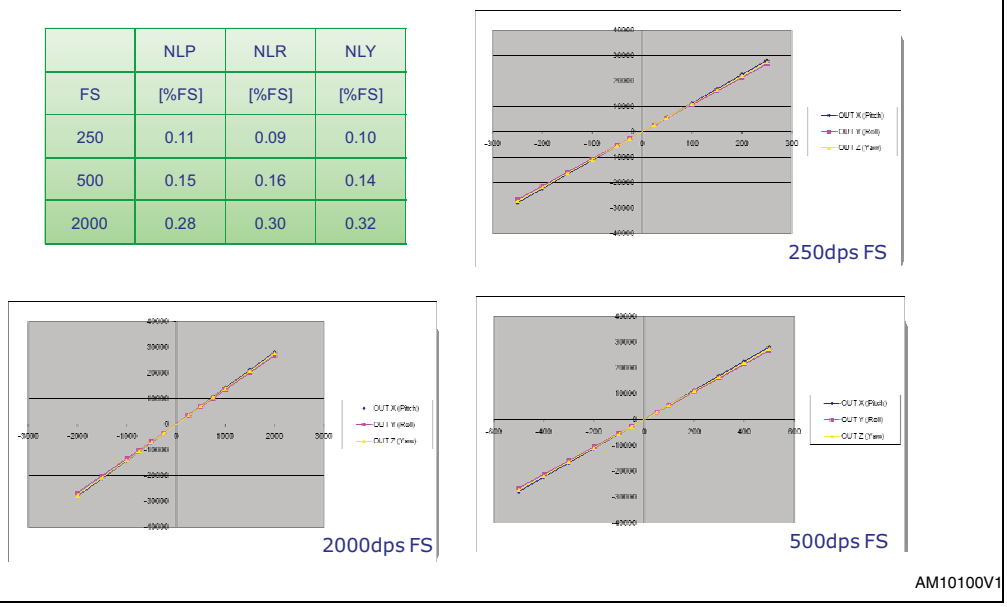

3.3 Zero-rate level change vs. temperature

This parameter defines how the zero-rate level or bias will change when the temperature changes. *Figure 7* and *8* show the characterization data based on 33 parts at 250 dps full-scale range, which demonstrates the high stability of the zero-rate level over temperature with tight distribution.

Figure 7. Zero-rate level vs. temperature characterization at 250 dps FS

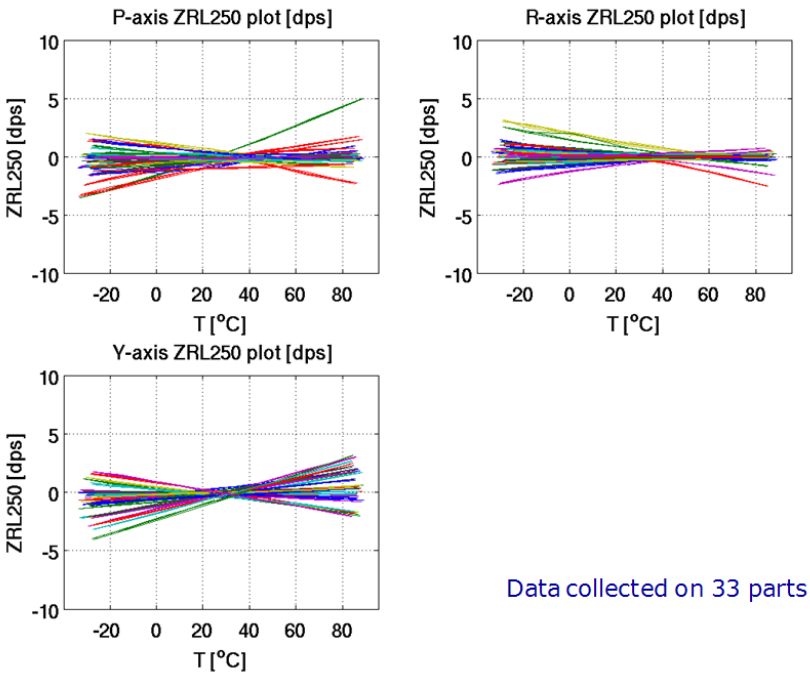

Figure 8. Zero-rate level vs. temperature distribution at 250 dps FS

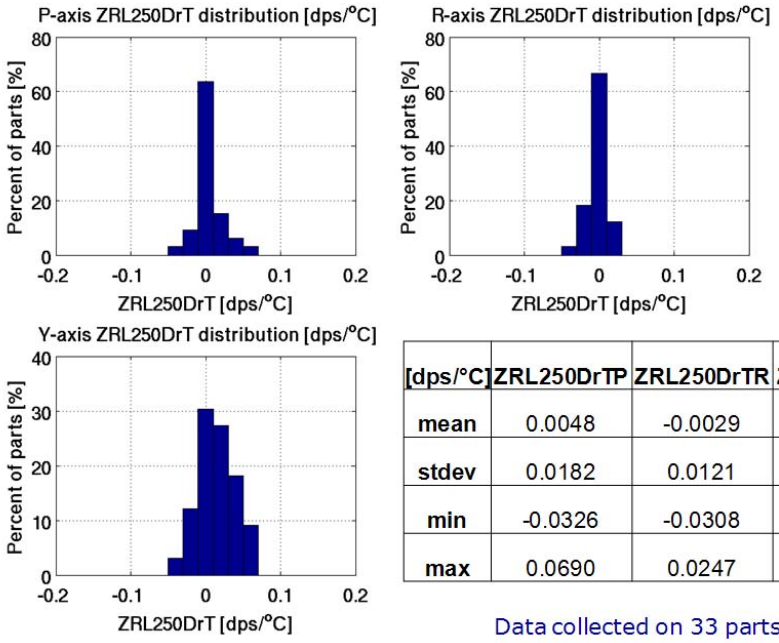

[dps/°C]	ZRL250DrTP	ZRL250DrTR	ZRL250DrTY
mean	0.0048	-0.0029	0.0125
stdev	0.0182	0.0121	0.0245
min	-0.0326	-0.0308	-0.0342
max	0.0690	0.0247	0.0635

In *Figure 8* it can be seen that the zero-rate level change is below 0.0125 dps/ °C on the yaw axis. This means that when the temperature changes 50°C from 25 °C to 75 °C, the zero-rate level change will be within 0.0125 dps/ °C * 50 °C = ±0.625 dps which is incredibly small.

Figure 9 and *10* show the characterization data based on 33 parts at 500 dps full-scale range and *Figure 11* and *12* show the characterization data based on 33 parts at 2000 dps full-scale range.

Figure 9. Zero-rate level vs. temperature characterization at 500 dps FS

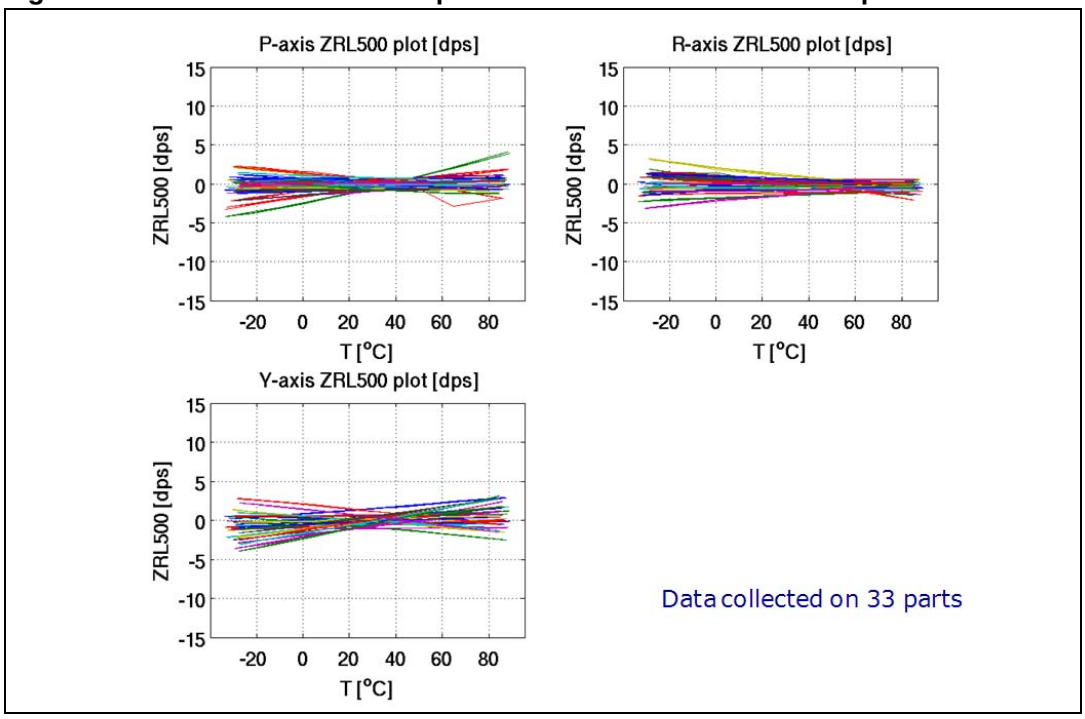

Figure 10. Zero-rate level vs. temperature distribution at 500 dps FS

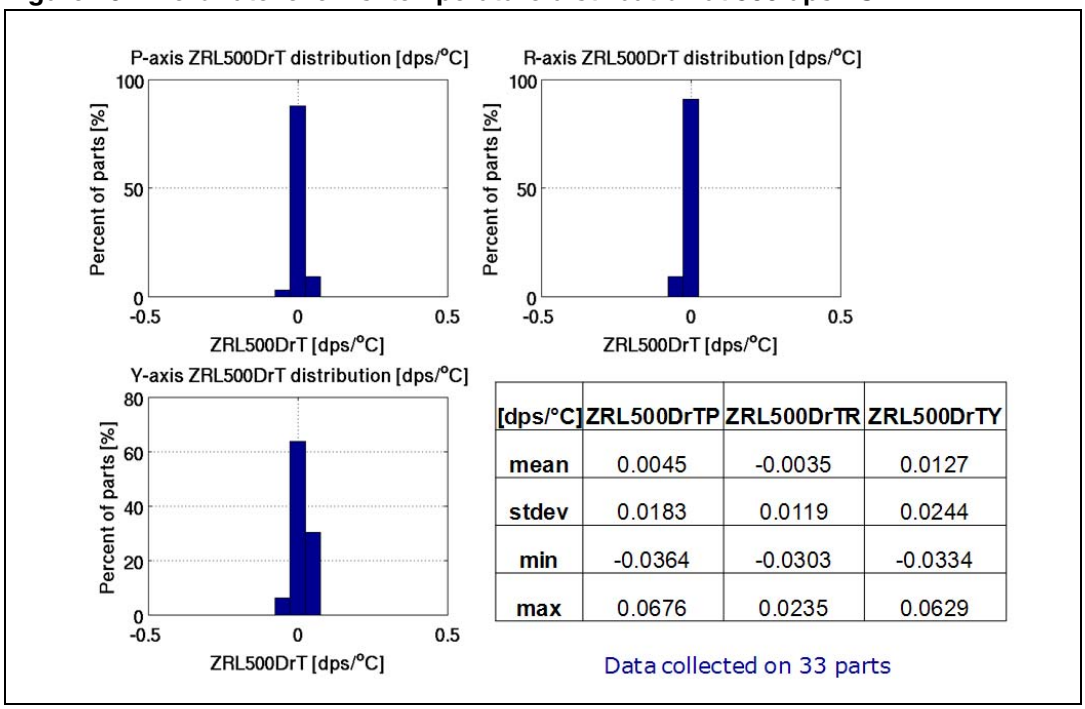

[dps/°C]	ZRL500DrTP	ZRL500DrTR	ZRL500DrTY
mean	0.0045	-0.0035	0.0127
stdev	0.0183	0.0119	0.0244
min	-0.0364	-0.0303	-0.0334
max	0.0676	0.0235	0.0629

Figure 11. Zero-rate level vs. temperature characterization at 2000 dps FS

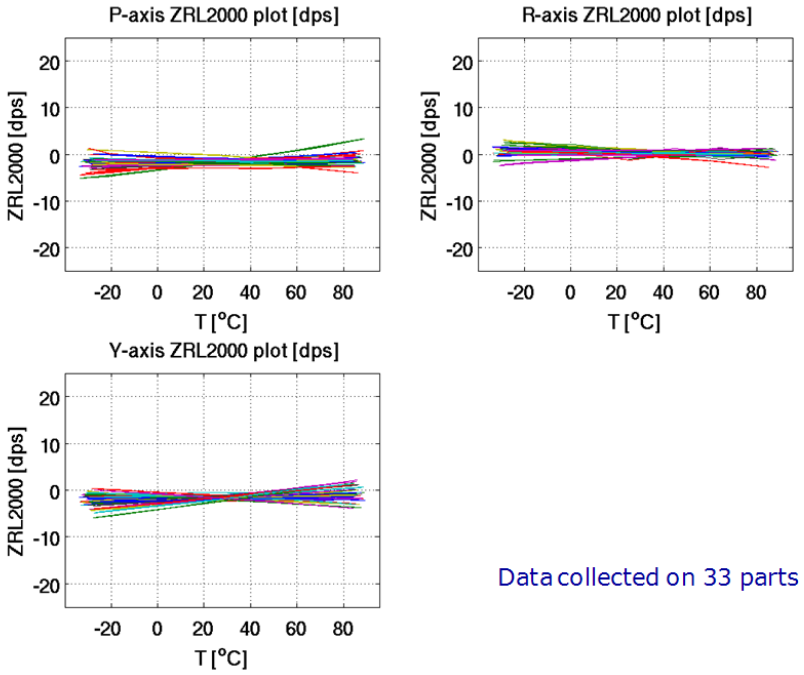

Figure 12. Zero-rate level vs. temperature distribution at 2000 dps FS

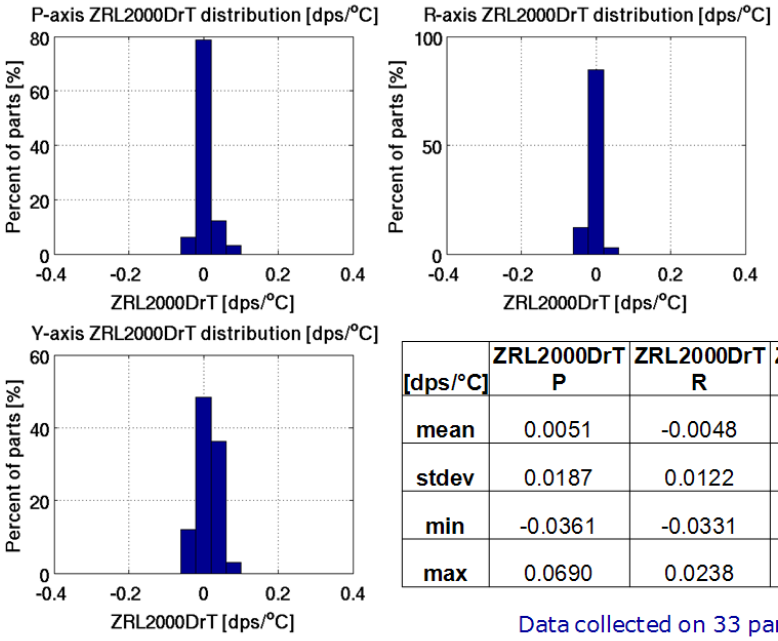

[dps/°C]	ZRL2000DrT P	ZRL2000DrT R	ZRL2000DrT Y
mean	0.0051	-0.0048	0.0137
stdev	0.0187	0.0122	0.0251
min	-0.0361	-0.0331	-0.0349
max	0.0690	0.0238	0.0668

Data collected on 33 parts

3.4 Sensitivity change vs. temperature

This parameter defines how the sensitivity or scale factor will change from the factory-trimmed sensitivity values when the temperature changes. *Figure 13* and *14* show the characterization data based on 22 parts at 250 dps full-scale range, which demonstrates ultra-high stability of the sensitivity over temperature with tight distribution.

In *Figure 14* it can be seen that the sensitivity change is 0.0301%/°C on the roll axis. This means that when the temperature changes 50°C from 25 °C to 75 °C, the sensitivity change will be within ±0.0301 %/°C * 50 °C = ±1.51% of the factory-trimmed sensitivity values. This deviation is ultra small.

Figure 13. Sensitivity vs. temperature characterization at 250 dps FS

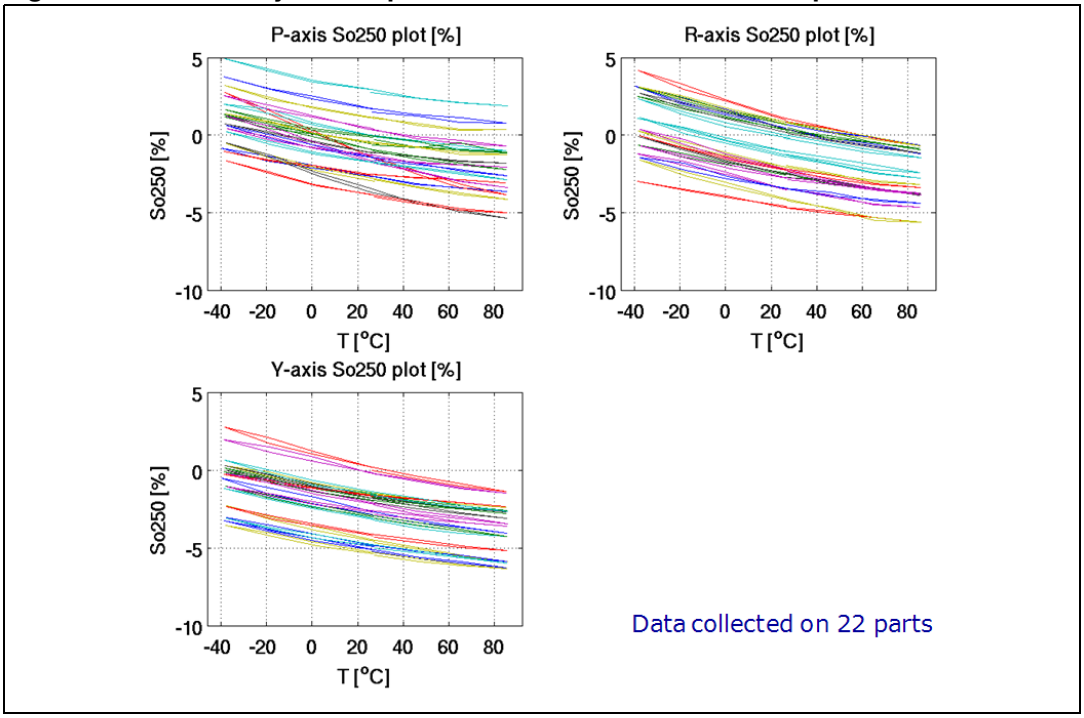

Figure 14. Sensitivity vs. temperature distribution at 250 dps FS

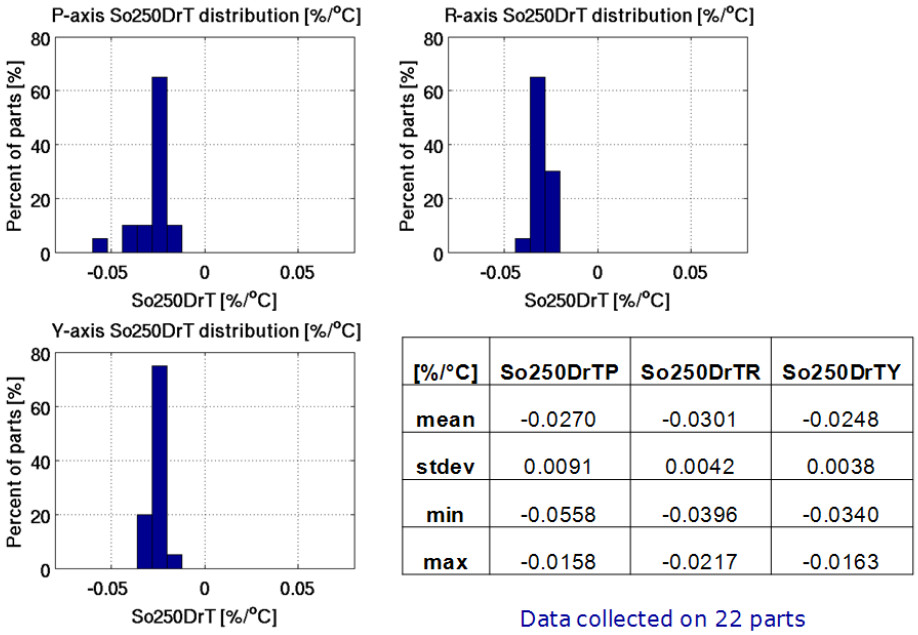

[%/°C]	So250DrTP	So250DrTR	So250DrTY
mean	-0.0270	-0.0301	-0.0248
stdev	0.0091	0.0042	0.0038
min	-0.0558	-0.0396	-0.0340
max	-0.0158	-0.0217	-0.0163

Figure 15 and *16* show the characterization data based on 22 parts at 500 dps full-scale range and *Figure 17* and *18* show the characterization data based on 22 parts at 2000 dps full-scale range.

Figure 15. Sensitivity vs. temperature characterization at 500 dps FS

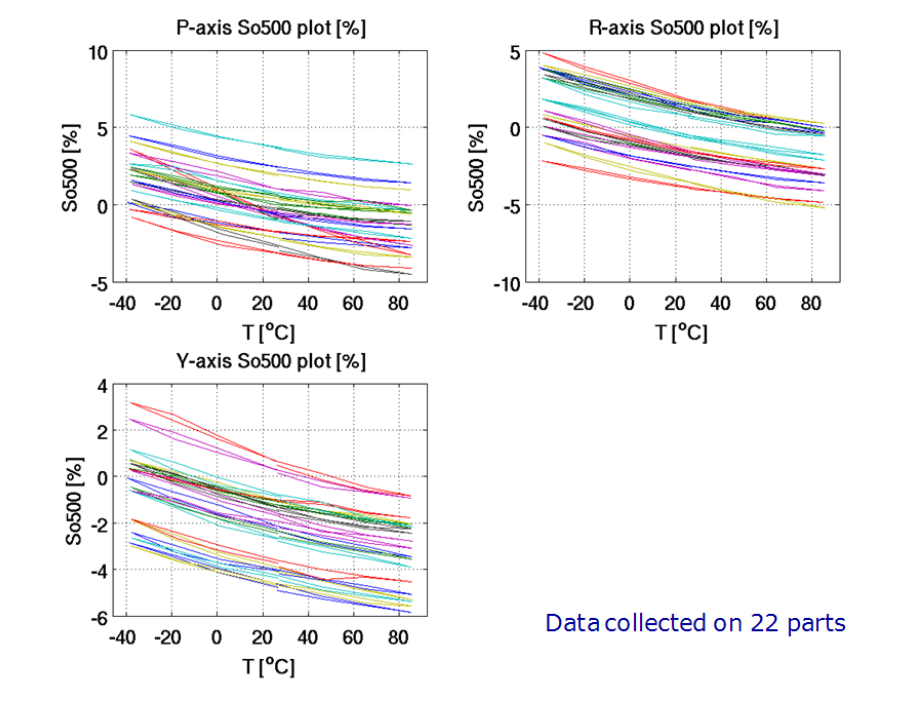

Figure 16. Sensitivity vs. temperature distribution at 500 dps FS

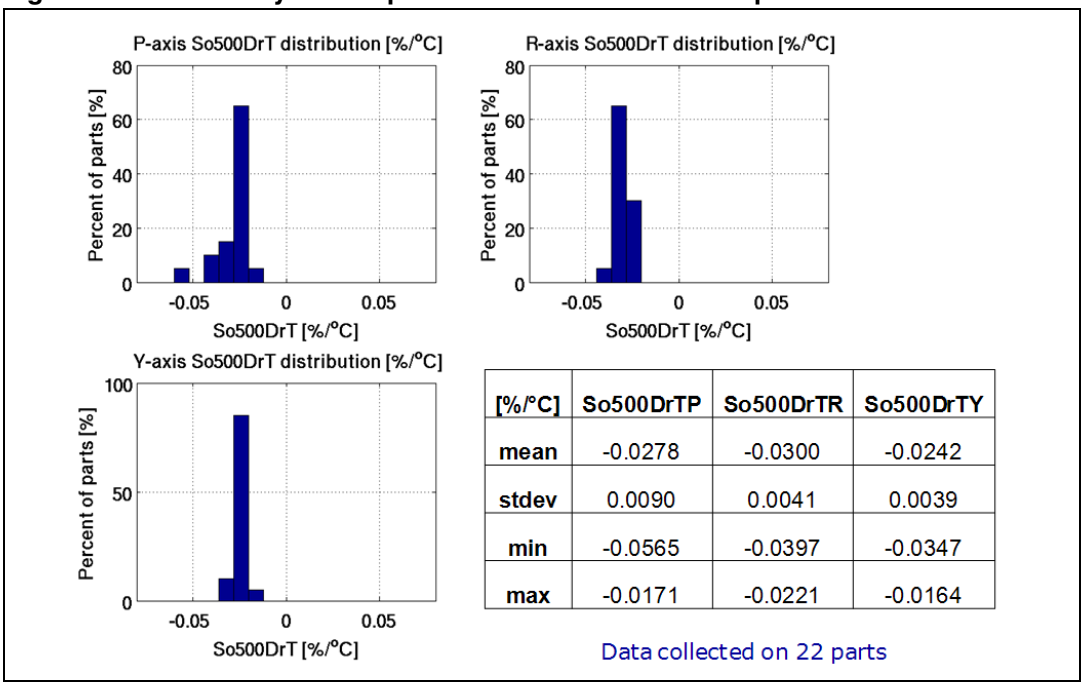

[%/°C]	So500DrTP	So500DrTR	So500DrTY
mean	-0.0278	-0.0300	-0.0242
stdev	0.0090	0.0041	0.0039
min	-0.0565	-0.0397	-0.0347
max	-0.0171	-0.0221	-0.0164

Figure 17. Sensitivity vs. temperature characterization at 2000 dps FS

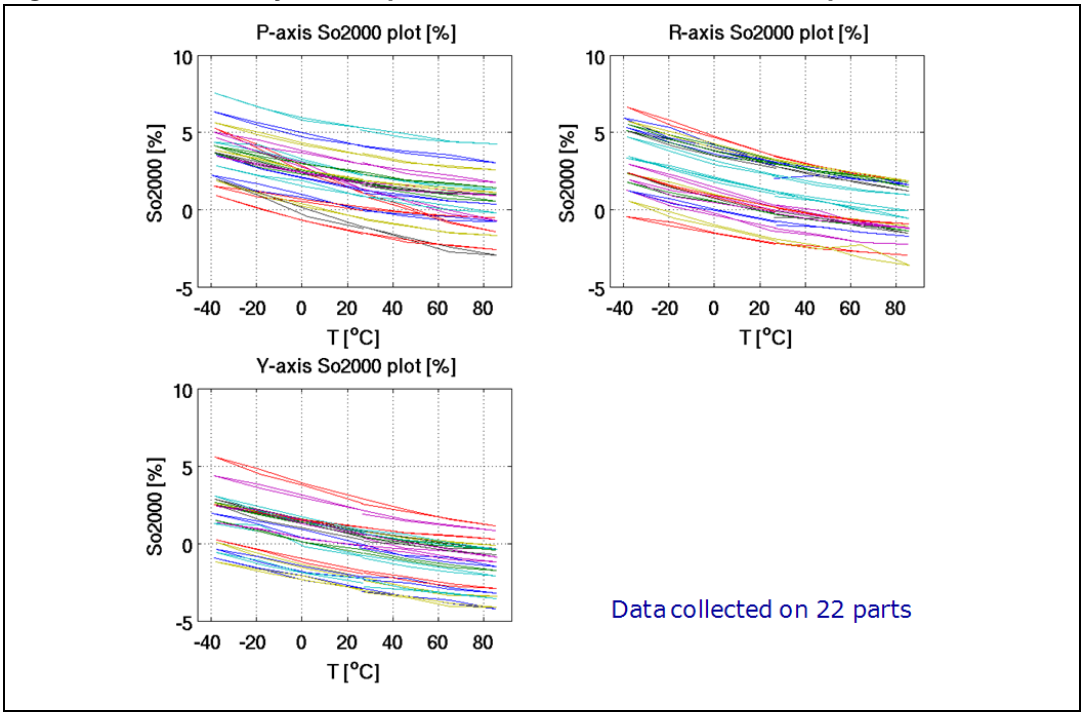

Figure 18. Sensitivity vs. temperature distribution at 2000 dps FS

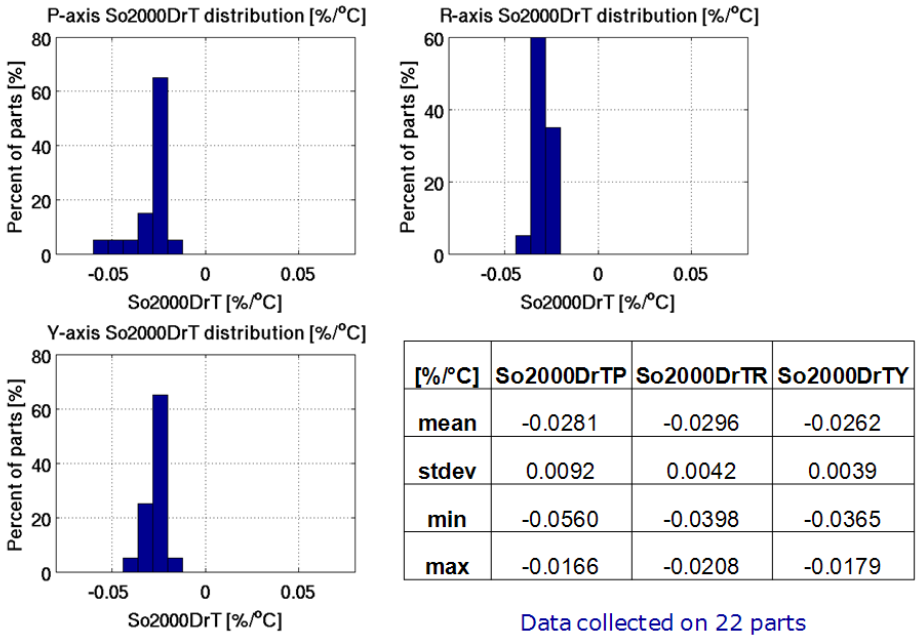

[%/°C]	So2000DrTP	So2000DrTR	So2000DrTY
mean	-0.0281	-0.0296	-0.0262
stdev	0.0092	0.0042	0.0039
min	-0.0560	-0.0398	-0.0365
max	-0.0166	-0.0208	-0.0179

3.5 Zero-rate level distribution part by part

Each gyroscope is factory tested and trimmed for zero-rate level. *Figure 19*, *20* and *21* show the zero-rate level distribution part by part over 1000 samples of parts at 250 dps, 500 dps and 2000 dps FS, respectively. It can be seen that the zero-rate level presents very narrow distribution which means each gyroscope has very little zero-rate level variation.

Figure 19. Zero-rate level distribution at 250 dps FS

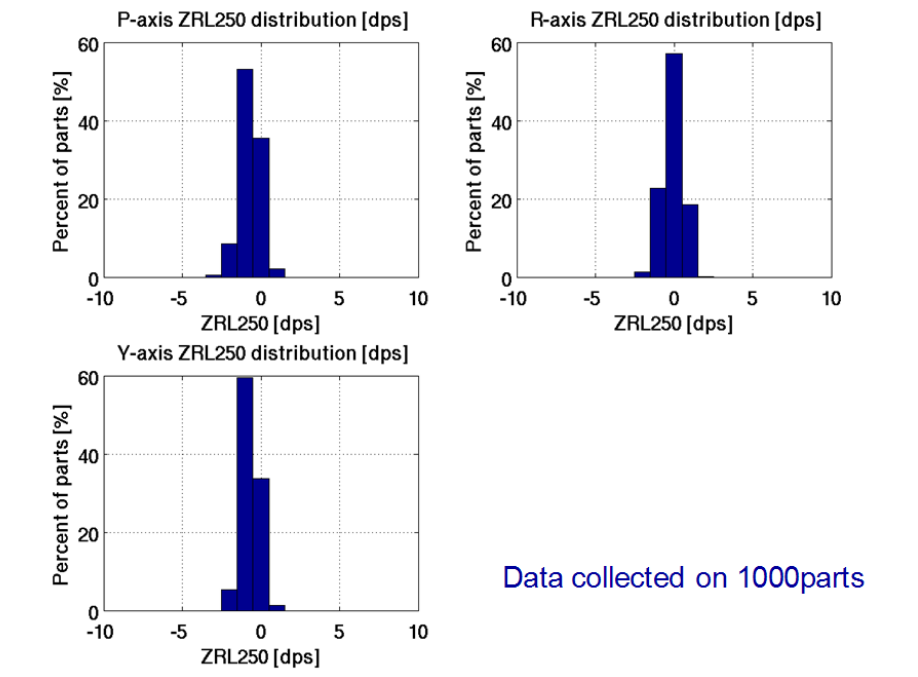

Figure 20. Zero-rate level distribution at 500 dps FS

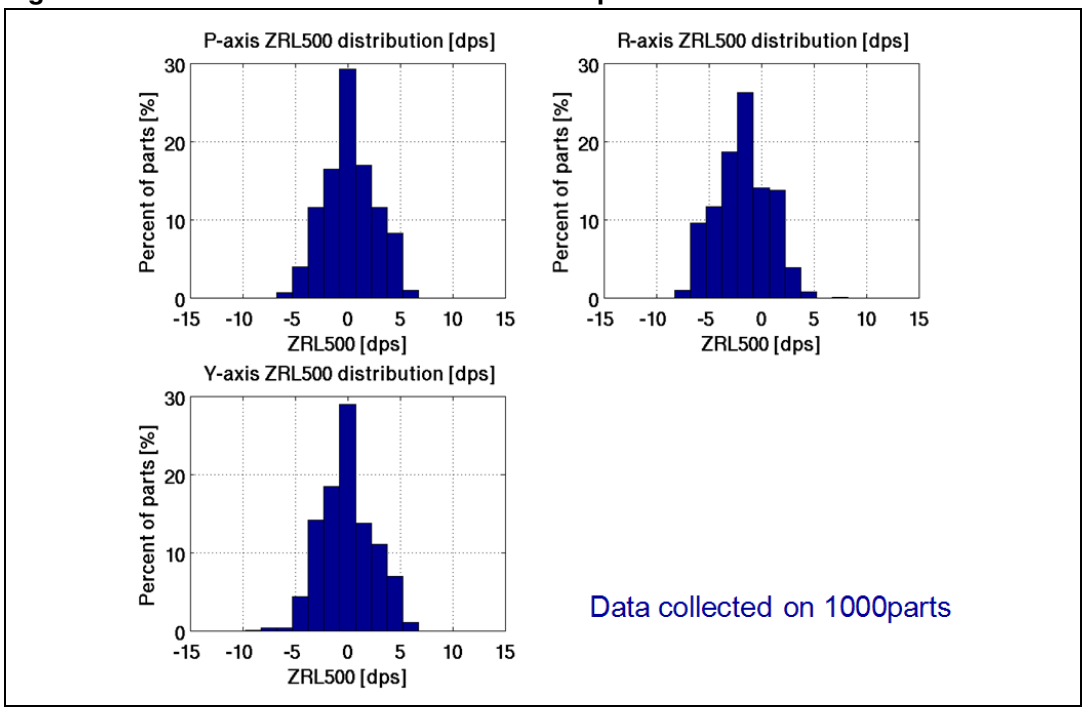

Figure 21. Zero-rate level distribution at 2000 dps FS

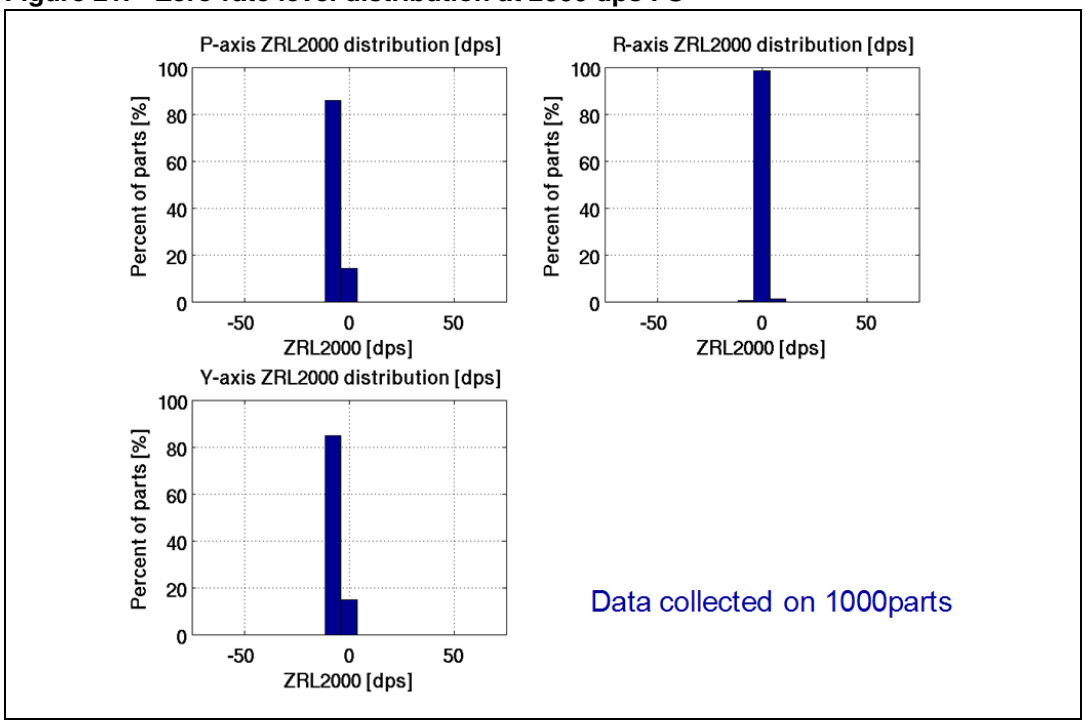

3.6 Sensitivity distribution part by part

Each gyroscope is factory tested and trimmed for sensitivity. *Figure 22* shows the sensitivity distribution part by part over 1000 samples of parts at 250 dps, 500 dps and 2000 dps FS. It can be seen that the sensitivity has very narrow distribution which means each gyroscope has very little sensitivity variation.

Figure 22. Sensitivity distribution

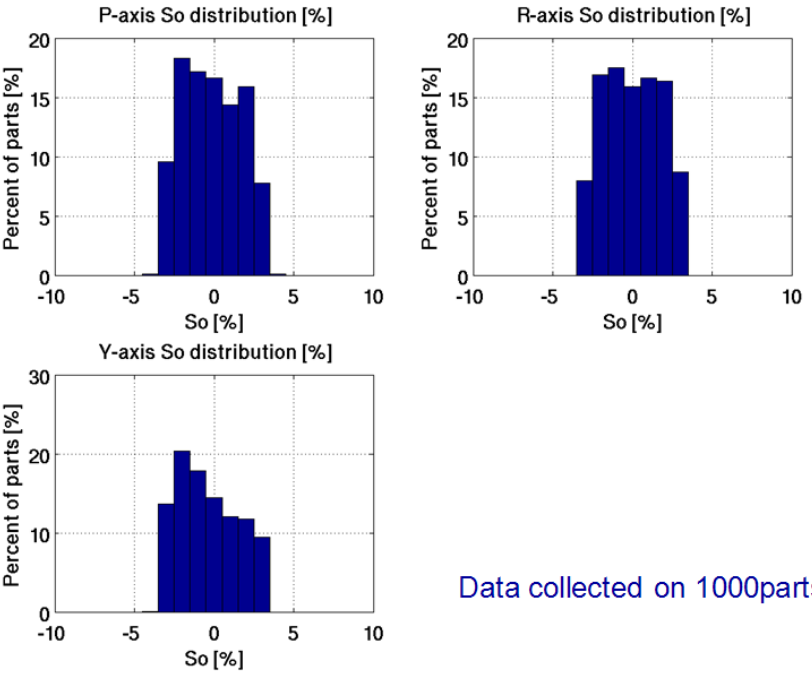

3.7 Rejection to acoustical noise

There are two main approaches to evaluate the acoustical noise rejection: white noise testing and sine wave testing.

White noise testing evaluates the effect of common environmental acoustical noise on the gyroscope's outputs. This is an effective method to analyze the gyroscope response to the environmental audio noise because the acoustical noise power is randomly distributed over all audio frequencies.

Sine wave testing focuses on gyroscope noise rejection characteristics when a theoretical worst condition is applied. When applied audio noise frequency is close to the gyroscope's driving frequency, the gyroscope's outputs will have the largest magnitude of coupled acoustical noise.

The setup for the two acoustical noise rejection tests consists of:

- A stereo loudspeaker which can generate white noise from 100 Hz to 10 kHz and sine tone at the gyroscope's driving frequency
- A reference microphone which can measure the acoustic magnitude to match the test specification
- A DUT board that has the gyroscope installed
- A National Instruments (NI) data acquisition system that can log raw data from the gyroscope
- An Agilent signal generator to generate the specified acoustic noise signal to the speaker

Figure 23 shows the acoustical white noise rejection characterization data based on 10 seconds of data acquisition. Then the standard deviation on the gyroscope's outputs is obtained to indicate the coupled noise from the acoustical white noise.

Figure 24 shows the acoustical sine wave noise rejection characterization data based on 10 seconds of data acquisition. Then the standard deviation on the gyroscope's outputs is obtained to indicate the coupled noise from the acoustical sine wave noise.

Figure 23. Acoustical white noise rejection characterization

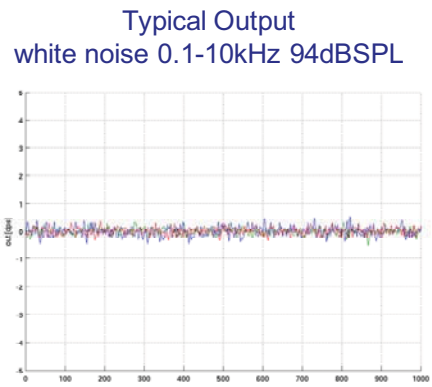

ODR 100Hz BW 12.5Hz

[dps]	X	Y	Z
dut1	0.164	0.117	0.126
dut2	0.14	0.105	0.113
dut3	0.16	0.135	0.121
dut4	0.128	0.113	0.11

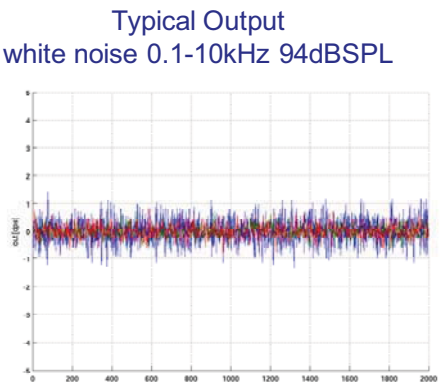

ODR 200Hz BW 50Hz

[dps]	X	Y	Z
dut1	0.414	0.22	0.245
dut2	0.32	0.196	0.219
dut3	0.439	0.28	0.256
dut4	0.256	0.227	0.22

AM10098V1

From *Figure 23*, it can be seen that the gyroscope noise standard deviation is below 0.17 dps at 100 Hz ODR with 12.5 Hz BW and below 0.44 dps at 200 Hz ODR with 50 Hz BW.

Figure 24. Acoustical sine wave noise rejection characterization

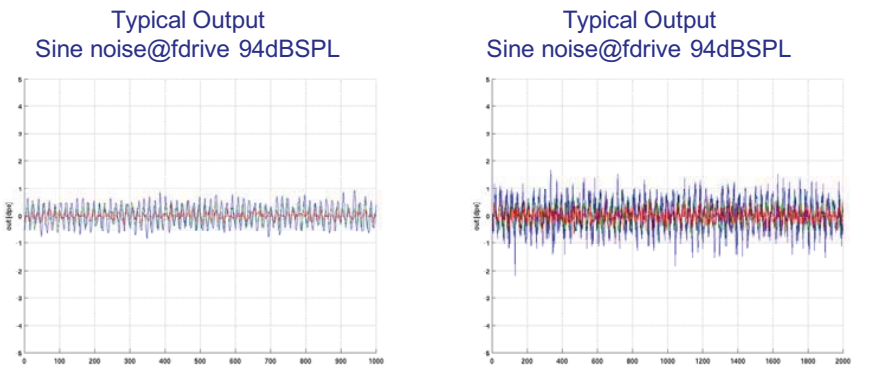

[dps]	X	Y	Z
dut1	0.388	0.251	0.114
dut2	0.529	0.16	0.131
dut3	0.655	0.258	0.141
dut4	0.723	0.187	0.14

AVE: 0.31 dps

[dps]	X	Y	Z
dut1	0.582	0.326	0.225
dut2	0.695	0.253	0.237
dut3	0.759	0.334	0.249
dut4	0.762	0.288	0.229

AVE: 0.41 dps

AM10099V1

From *Figure 24*, it can be seen that the gyroscope noise standard deviation is below 0.31dps at 100 Hz ODR with 12.5Hz BW and below 0.41dps at 200 Hz ODR with 50 Hz BW.

4 Comparing ST's gyroscopes to the competition

Comparing the datasheets from 3-axis MEMS digital gyroscopes from ST to the current solutions on the market, ST's gyroscopes have much better performance in terms of zero-rate level and sensitivity over temperature. In addition, there are also two main advantages of ST's gyroscopes: resistance to external stress and lower noise density level.

4.1 Resistance to external stress

The patented Mushroom design in ST's MEMS gyroscopes allows excellent resistance to external mechanical forces as shown in *Figure 25*. In order to measure ST's performance against that of a competitor, dedicated comparison tests have been performed under identical setup and conditions.

Figure 25. Comparison of resistance to external stress

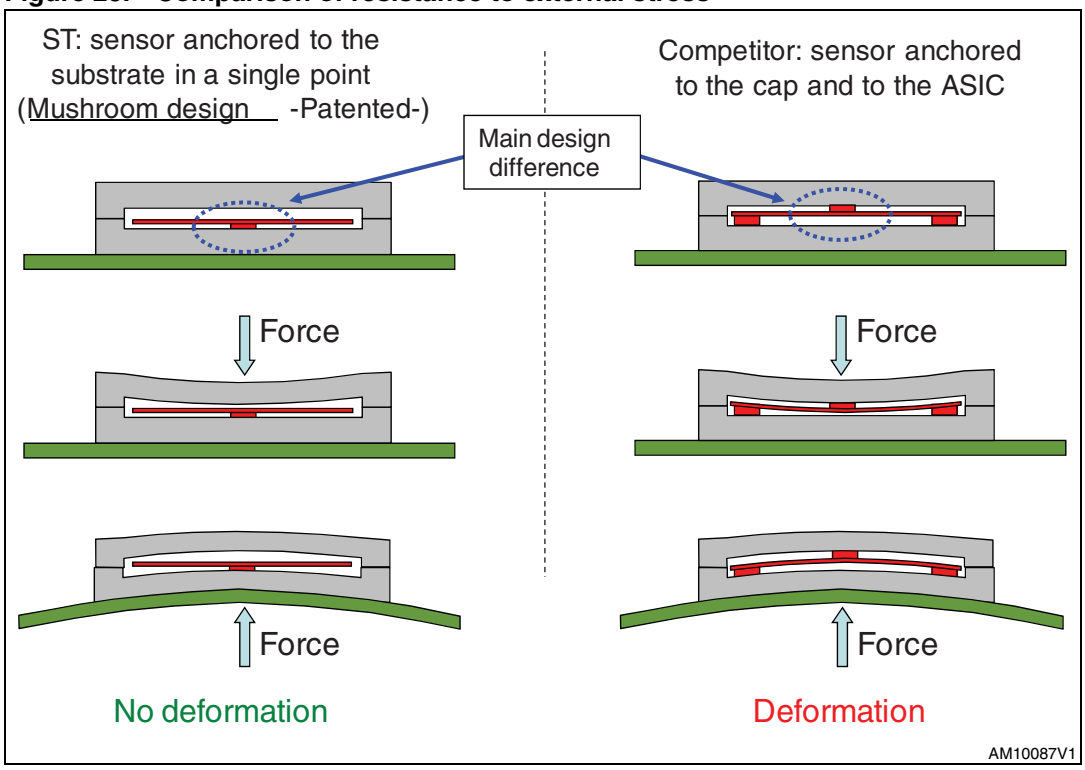

Figure 26. Comparison of the performance under external stress

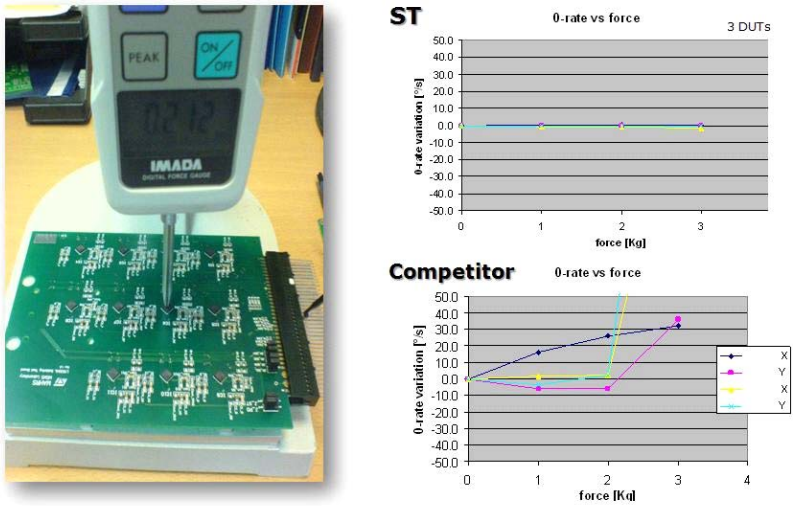

After the PCB is mounted inside a handheld device, some form of stress is always acting on the device. Additionally, when end users are holding the handheld devices to play games, the external stress changes. Therefore, it is very important to make the gyroscopes immune to the changes in external force in order to maintain constant and robust performance as shown in *Figure 26*.

Figure 26 clearly demonstrates the ST gyroscope's outstanding performance while the device is subjected to a force up to 3 kg applied on the package. Other solutions currently on the market show that under the same external mechanical stress, the gyroscope output reaches high values, preventing correct behavior of the sensor and adversely affecting the gaming experience for the end user.

4.2 Lower noise density level

As mentioned before in *Section 2: The beauty of the MEMS single driving structure design*, when using three single structures or one single, plus one dual structure at different driving frequencies, by nature the mismatch between driving frequencies will cause spurious noise on the gyroscope's output signals. The high level of symmetry in the single driving structure design allows ST's gyroscopes to have much lower noise density than the competitor's gyroscope as shown in *Figure 27*.

Figure 27. Comparison of noise density level from an Allan Variance plot

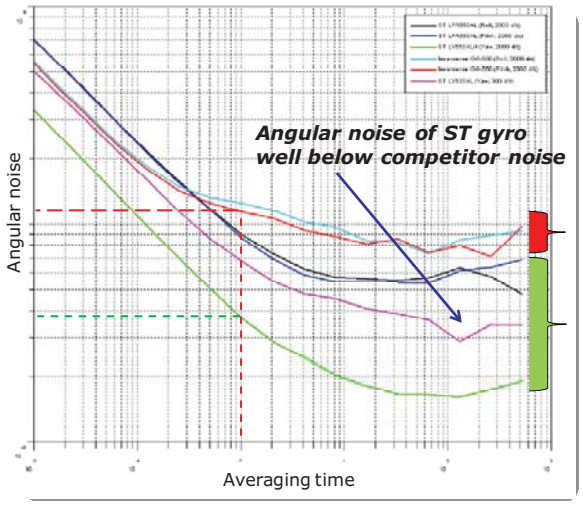

5 Getting started with ST's 3-axis digital gyroscope

This section will use ST's L3G4200D 3-axis MEMS digital gyroscope as an example to show how to design it in various applications and then how to convert the gyroscope's raw data into meaningful angular velocity and angular displacement values.

5.1 Hardware design

The L3G4200D is a 4 x 4 x 1.1mm, 3-axis digital gyroscope that has 16-bit data output through the I^2C or SPI interface[2]. It has a full-scale range of ±250/±500/±2000 dps and an output data rate of 100/200/400/800 Hz user-selectable on the fly. The power supply Vdd to L3G4200D should be regulated from 2.4 V to 3.6 V, while the digital IO Vdd_IO can be powered from 1.71 V to Vdd + 0.1 V. For example, if the microprocessor is powered by 1.8 V and it can only accept a maximum of 1.8 V on its I/O pins, then 1.8 V can be used to power Vdd_IO on the L3G4200D gyroscope to make them compatible.

Figure 28 shows the typical hardware connections between the L3G4200D and a microprocessor.

Figure 28. Typical hardware connections for L3G4200D

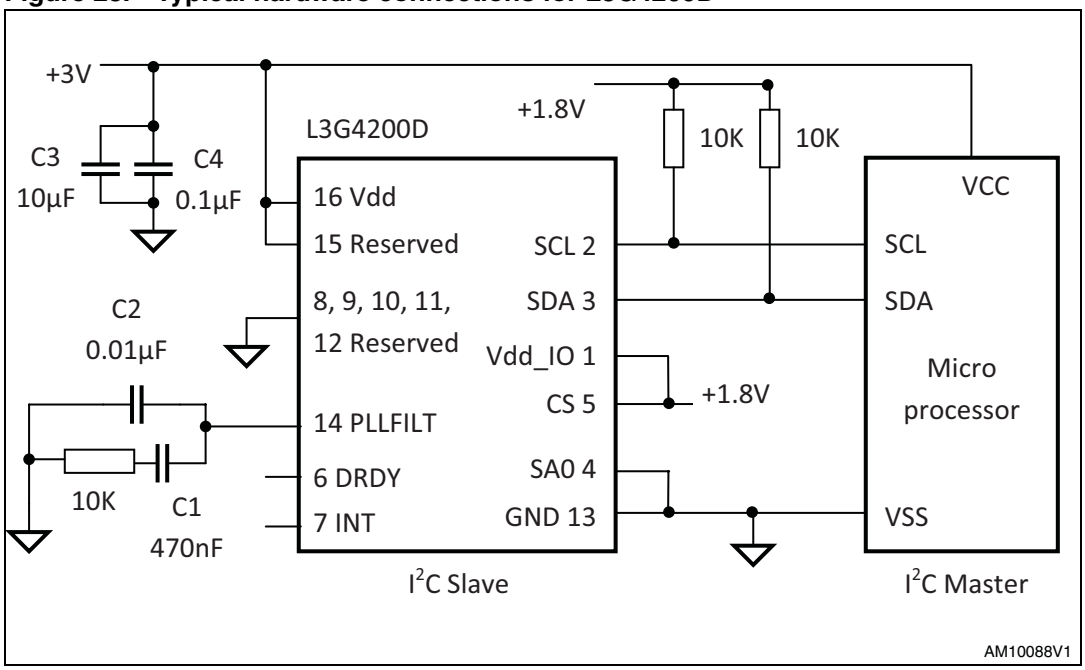

The L3G4200D is the I^2C slave and the microprocessor is the I^2C master. When designing the PCB layout, the following points should be considered:

- Capacitors C1 to C4 can be ceramic X7R or X5R capacitors with 6.3 V ratings and 10% tolerance
- Capacitor C1, C2 and 10 KOhms resistor (1% tolerance) are mandatory for the L3G4200D internal driving structure
- Power supply decoupling ceramic capacitors C3 (10 µF) and C4 (0.1 µF) should be placed as close as possible to the Vdd pin 6
- Choose a microprocessor that has a built-in I^2C controller. If a bit-banging scheme implemented in the microprocessor's firmware is used, pay attention to the I^2C communication timing specifications.
- If +2.5 V or +3 V or +3.3 V Vdd is OK for the microprocessor, then the +1.8 V Vdd_IO power supply can be tied to Vdd directly for a single power supply solution.
- Make sure there are no traces right beneath the L3G4200D on your PCB
- When designing the PCB layout, please refer to the LGA package surface mounting guidelines[3].

5.2 How to get meaningful information

Assuming that the above hardware design is done and your microprocessor is able to get the gyroscope's raw data in LSBs through the I^2C or SPI interface, then the next step is converting the raw data into meaningful angular velocity values.

Please note that the 16-bit gyroscope's output data are in 2's complement format (signed integer) and the typical sensitivity at ±250 dps is 0.00875 dps/LSB from the datasheet. For example, when the gyroscope is stationary, the X-, Y- and Z-axis outputs may look like the following:

X-axis: FF96 LSBs = -106 LSBs = -106 * 0.00875 = -0.93 dps

Y-axis: 0045 LSBs = 69 LSBs = 69 * 0.00875 = 0.6 dps

Z-axis: FFCC LSBs = -52 LSBs = -0.46 dps

Therefore, the MEMS gyroscope output can be expressed as shown in *Equation 2:*

Equation 2

$$R_t = SC * (R_m - R_0)$$

where,

- R_t is the true angular rate given in dps
- R_m is the MEMS gyroscope measurement given in signed integer LSBs
- R_0 is the zero-rate level given in signed integer LSBs (the gyroscope output when no angular rate is applied)
- SC is the scale factor (or sensitivity) given in dps/LSB

In order to compensate for turn-on to turn-on bias instability, after the gyroscope is powered on, the user can collect 50 to 100 samples and then average these samples as the turn-on zero-rate level R_0 assuming that the MEMS gyroscope is stationary. For example, if the gyroscope ODR is set to 100 Hz, then this process only takes about 0.5 to 1 seconds. All the subsequent gyroscope readings can then subtract this turn-on zero-rate level R_0 as signed

integers. Due to the noise from the gyroscope output, a moving-average filtering method can be used to reduce the noise.

Due to the temperature change and measurement noise, MEMS gyroscope readings will vary slightly when the gyroscope is at rest. It is necessary to set a threshold R_{th} to zero the gyroscope readings if the absolute value is within that threshold as shown in *Equation 3*. This will get rid of the zero-rate noise so that the angular displacement will not accumulate when the gyroscope is stationary. The threshold can be determined as 3-sigma of the standard deviation of the gyroscope measurements when no angular velocity is applied to any sensing axis of the gyroscope. The disadvantage of this threshold is that the gyroscope will ignore very slow rotation speeds within that threshold.

Equation 3

$$\Delta R = (R_m - R_0) = 0 \qquad \text{if } |(R_m - R_0)| < R_{th}$$

Every few minutes, whenever the MEMS gyroscope is at rest, the user always can sample 50 to 100 gyroscope data and then average these samples as the new zero-rate level R_0. This will eliminate the zero-rate in-run bias and small temperature change.

With the above consideration *Equation 2* becomes:

Equation 4

$$R_t = SC * (R_m - R_0) = SC * \Delta R$$

Applied to the 3-axis digital gyroscope L3G4200D, the true angular on the X-, Y- and Z-axis will be,

Equation 5

$$\begin{bmatrix} R_x \\ R_y \\ R_z \end{bmatrix} = \begin{bmatrix} SC_x & 0 & 0 \\ 0 & SC_y & 0 \\ 0 & 0 & SC_z \end{bmatrix} * \begin{bmatrix} R'_x - R_{x0} \\ R'_y - R_{y0} \\ R'_z - R_{z0} \end{bmatrix}$$

where,

- R'_x, R'_y, R'_z, are the raw measurements of the gyroscope,
- R_{x0}, R'_{y0}, R'_{z0}, are the zero-rate level or bias on each axis,
- SC_x, SC_y, SC_z, are the scale factor or sensitivity of each axis,
- R_x, R_y, R_z, are the final angular velocity information of each axis

So the next step will be to determine the scale factor SC_x, SC_y, SC_z in *Equation 5* by using a reference system. After the calibration, the scale factor parameters should be saved in non-volatile memory for future use. Please note that the gyroscope's sensitivity usually is very stable over time and temperature and this calibration is needed only for highly sensitive applications.

The gyroscope's measurements have positive and negative values. If the applied angular velocity along one sensing axis is counterclockwise, then the gyroscope of that sensing axis will output positive values. If the applied angular velocity is clockwise around the sensing axis, then the gyroscope of that sensing axis will output negative values (represented by the blue curves in *Figure 29*).

Figure 29. L3G4200D output signal on the Z-axis (yaw angular rate applied)

Integrating the blue curves over time gives the angular displacement or how many degrees rotated. The following sample code shows how to calculate the angular displacement on one axis of the gyroscope output in digital domain.

$\Delta x = 0;$

while (1)

{ $\Delta x = \Delta x + h * Rx * SCx);$}

where,

- Δx is the gyroscope's angular displacement on the X-axis given in degrees
- h is the sampling period given in seconds. If ODR = 100 Hz, then h = 0.01 s
- R_x is gyroscope's raw data given in LSBs after removal of the zero-rate level offset and the threshold
- SC_x is the scale factor of the gyroscope's X-axis given in dps/LSB

5.3 Gyroscope calibration

Each L3G4200D is factory tested and trimmed for zero-rate level and sensitivity. So for most common applications such as gaming or air mouse pointing devices, no further calibration is required. Users can simply use the typical sensitivity values from the datasheet to convert the gyroscope's raw data to meaningful angular velocity or angular displacement as explained in *Section 5.2: How to get meaningful information*.

However, after the 3-axis digital gyroscope L3G4200D is installed on a PCB and the PCB is mounted inside a handheld device such as a PDA, the sensing axes X, Y and Z of the gyroscope are invisible. The only visible axes are the handheld device body axes X_b, Y_b and Z_b. If the PCB has any misalignment with respect to the handheld body axes, then the

angular velocity that is only applied to the Z_b axis of the handheld will have projection on the X_b and Y_b axis of the handheld body axes. Therefore, it is necessary to find the misalignment matrix to compensate the gyroscope measurements. Then *Equation 5* becomes,

Equation 6

$$\begin{bmatrix} R_x \\ R_y \\ R_z \end{bmatrix} = G\_m_{3x3} \begin{bmatrix} SC_x & 0 & 0 \\ 0 & SC_y & 0 \\ 0 & 0 & SC_z \end{bmatrix} * \begin{bmatrix} R'_x - R_{x0} \\ R'_y - R_{y0} \\ R'_z - R_{z0} \end{bmatrix}$$

$$= \begin{bmatrix} G_{11} & G_{12} & G_{13} \\ G_{21} & G_{22} & G_{23} \\ G_{31} & G_{32} & G_{33} \end{bmatrix} * \begin{bmatrix} R'_x - G_{10} \\ R'_y - G_{20} \\ R'_z - G_{30} \end{bmatrix}$$

So the gyroscope calibration is to determine the above 12 parameters by using a single-axis rate table or a step-motor spin table as shown in *Figure 30*.

Figure 30. Gyroscope calibration setup

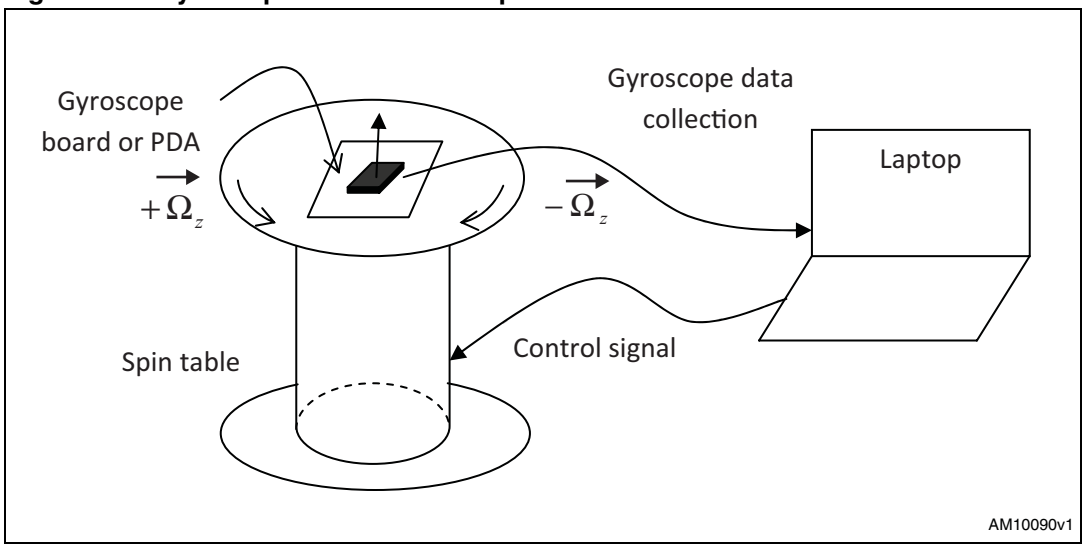

Calibration procedure example

1. Mount the gyroscope's PC board, or a PDA that has gyroscope installed, on the leveled top surface of the spin table. In order to measure the gyroscope's raw data along the X- and Y-axis, mount the PC board or PDA inside an orthogonal aluminum cube.
2. Power on the gyroscope and wait a few minutes for it to warm up.
3. Collect 100 samples of gyro data and then average those samples as the zero-rate level R_{x0}, R_{y0}, R_{z0}.
4. Let the spin table start spinning counterclockwise at R_z = +50 dps and $R_x = R_y$ = 0 dps (top view).
5. Wait until the spin table angular velocity becomes stable. Then start collecting the gyroscope's raw data for one full round.
6. Stop the spin table.
7. Let the spin table start spinning clockwise at R_z = -50 dps and $R_x = R_y$ = 0 dps. Then repeat steps (5) and (6) to collect the gyroscope's raw data.
8. Let the spin table start spinning counterclockwise at R_z = +100 dps and $R_x = R_y$ = 0 dps. Then repeat steps (5) and (6) to collect the gyroscope's raw data.
9. Let the spin table start spinning clockwise at R_z = -100 dps and $R_x = R_y$ = 0 dps. Then repeat steps (5) and (6) to collect the gyroscope's raw data.
10. Flip around the aluminum cube so that the X-axis is facing up on the spin table. Then repeat steps (4) to (9) to collect the gyroscope's raw data along the X-axis.
11. Flip around the aluminum cube so that the Y-axis is facing up on the spin table. Then repeat steps (4) to (9) to collect the gyroscope's raw data along the Y-axis.
12. Gyroscope calibration is done.
13. Construct the known applied angular rate data into a matrix and construct the gyroscope's raw data into another matrix. Then apply the Least Squares method to determine the 12 calibration parameters.

6 Gyroscope-enabled gaming and navigation

After the gyroscope calibration, the user can correctly convert the gyroscope's raw data to angular velocity in dps around X_b, Y_b and Z_b of the handheld body axes. This section will give an example on how to control an object in the handheld device for motion-enabled gaming and the mathematical equations for navigation.

6.1 Gyroscope-enabled gaming control

MEMS accelerometers have been widely used in handheld devices for screen portrait/landscape applications and simple motion gaming control. However, there are some limitations for accelerometer-enabled motion games because the accelerometer is only suitable for static tilt measurements or slow motion applications. In order to control a teapot as shown in *Figure 31*, it is impossible for the accelerometer to rotate the teapot when the handheld device is rotating on a horizontal plane. In addition, when tilting the handheld device very fast, the tilt measurement from the accelerometer cannot follow the dynamic motion so the user does not have a good feeling of control.

With the 3-axis gyroscope, the above issues are solved because the gyroscope can measure the dynamic angular velocity which gives the user a more responsive and smooth feeling when playing gameswith the handheld device. Regardless of the rotation of the handheld device in 3D space, the 3-axis gyroscope can continuously give the angular velocity measurement around 3 axes.

Therefore, the solution for gaming control could be as follows:

- At any arbitrary 3D position of the handheld device, when the game is launched, manually set pitch, roll and yaw to 0 degree.
- Whenever the handheld device is rotating, the teapot will rotate correspondingly, based on the gyroscope's measurements of the X/Y/Z-axis.
- Whenever the handheld device rotation is stopped, the teapot will stay at the current orientation because the gyroscope's measurements of the X/Y/Z-axis will be 0 LSBs.

Figure 31. Motion gaming in handheld devices

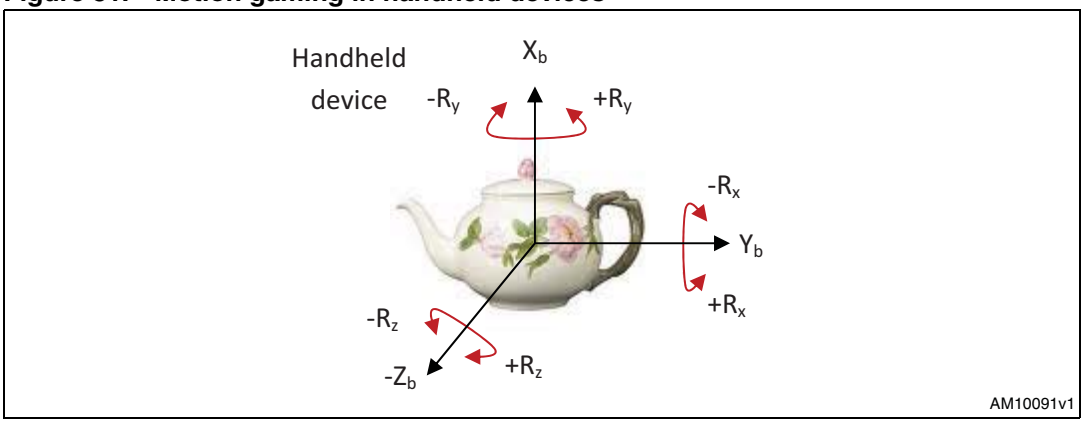

6.2 Gyroscope-enabled navigation

In strapdown inertial navigation theory [4], a 3-axis accelerometer and 3-axis gyroscope are used as a 6D IMU. The purpose of the gyroscope is to construct the direct cosine matrix (DCM) between the handheld device body axes and the local horizontal frame. Then the accelerometer measurements on the body axes will be projected to the local horizontal plane from the DCM. Single integration of the projected acceleration will give the velocity of the handheld device and double integration will give the distance travelled for the handheld device. This section will discuss how to use gyroscope's measurements to construct the direct cosine matrix.

Three Euler angles are referenced to the local horizontal plane which is perpendicular to the earth's gravity. Users can define the handheld body axes as forward-right-down b-frame.

Yaw (ψ) is defined as the angle between the X_b axis and the initial orientation of the object on the horizontal plane, measured in clockwise direction when viewing from the top of the device.

Pitch (ρ) is defined as the angle between the X_b axis and the horizontal plane. When rotating the device around the Y_b axis with the X_b axis moving upwards, pitch is positive and increasing.

Roll (γ) is defined as the angle between the Y_b axis and the horizontal plane. When rotating the device around the X_b axis with the Y_b axis moving downwards, roll is positive and increasing.

Users also can define a local horizontal n-frame with the X- and Y-axis leveled and the Z-axis pointing down. Assuming that at the beginning, the handheld device body axes' b-frame is the same as the local horizontal n-frame. When the handheld device is at any arbitrary position in 3D space, three rotations can be applied to rotate the local horizontal n-frame to the handheld body current axes as shown below.

Firstly, rotate the handheld device around the Z_b axis clockwise at an angle (ψ) with view from the origin to downwards. Then rotate the device around Y_b at an angle (ρ) with X_b moving upwards. Then rotate the device around X_b at an angle (γ) with Y_b moving downwards. The new device body axes become X'_b, Y'_b and Z'_b as shown in *Figure 32*.

Then each rotation matrix is:

Equation 7

$$R_\psi = \begin{bmatrix} \cos\psi & \sin\psi & 0 \\ -\sin\psi & \cos\psi & 0 \\ 0 & 0 & 1 \end{bmatrix}$$

Equation 8

$$R_\rho = \begin{bmatrix} \cos\rho & 0 & -\sin\rho \\ 0 & 1 & 0 \\ \sin\rho & 0 & \cos\rho \end{bmatrix}$$

Equation 9

$$R_\gamma = \begin{bmatrix} 1 & 0 & 0 \\ 0 & \cos\gamma & \sin\gamma \\ 0 & -\sin\gamma & \cos\gamma \end{bmatrix}$$

So the relationship between $X'_b/Y'_b/Z'_b$ and $X_b/Y_b/Z_b$ is:

Equation 10

$$\begin{bmatrix} X'_b \\ Y'_b \\ Z'_b \end{bmatrix} = R_\gamma R_\rho R_\psi \begin{bmatrix} X_b \\ Y_b \\ Z_b \end{bmatrix}$$

$$= \begin{bmatrix} \cos\rho\cos\psi & \cos\rho\sin\psi & -\sin\rho \\ \cos\psi\sin\rho\sin\gamma - \cos\gamma\sin\psi & \cos\gamma\cos\psi + \sin\rho\sin\gamma\sin\psi & \cos\rho\sin\gamma \\ \cos\psi\sin\rho\cos\gamma + \sin\gamma\sin\psi & -\sin\gamma\cos\psi + \sin\rho\cos\gamma\sin\psi & \cos\rho\cos\gamma \end{bmatrix} \cdot \begin{bmatrix} X_b \\ Y_b \\ Z_b \end{bmatrix}$$

Figure 32. Rotation procedures

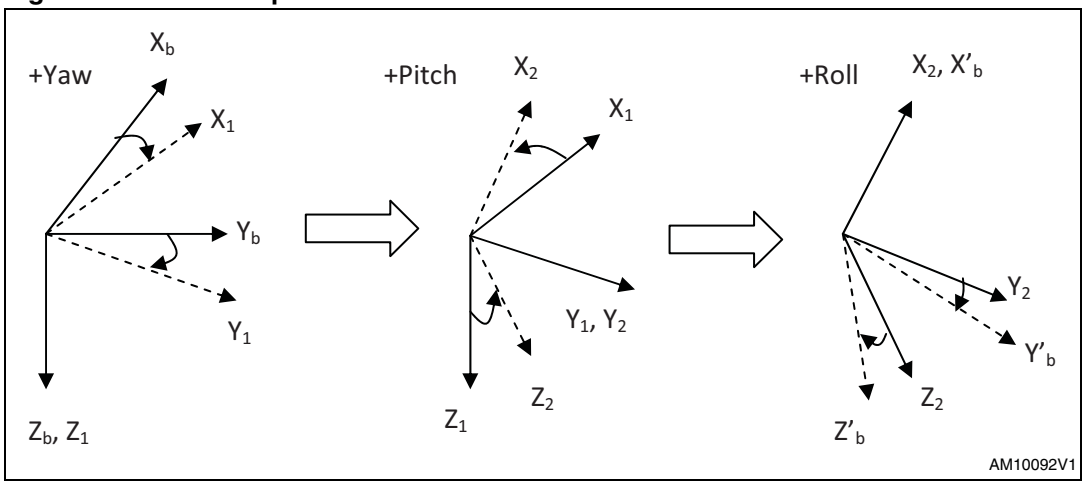

Therefore, the direct cosine matrix (DCM) from the body axes to the local horizontal n-frame will be [4]:

Equation 11

$$C_b^n = \begin{bmatrix} \cos\rho\cos\psi & \cos\psi\sin\rho\sin\gamma - \cos\gamma\sin\psi & \cos\psi\sin\rho\cos\gamma + \sin\gamma\sin\psi \\ \cos\rho\sin\psi & \cos\gamma\cos\psi + \sin\rho\sin\gamma\sin\psi & -\sin\lambda\cos\psi + \sin\rho\cos\gamma\sin\psi \\ -\sin\rho & \cos\rho\sin\gamma & \cos\rho\cos\gamma \end{bmatrix}$$

$$= \begin{bmatrix} C_{11} & C_{12} & C_{13} \\ C_{21} & C_{22} & C_{23} \\ C_{31} & C_{32} & C_{33} \end{bmatrix}$$

then,

Equation 12

$$\text{Pitch}(\rho) = \arcsin(-C_{31})$$
$$\text{Roll}(\gamma) = \arctan\left(\frac{C_{32}}{C_{33}}\right)$$
$$\text{Yaw}(\psi) = \arctan\left(\frac{C_{21}}{C_{11}}\right)$$

The quaternion is a four-parameter representation based on the idea that a transformation from one frame to another may be affected by a single rotation about a vector defined with respect to the reference frame [4].

Equation 13

$$q = \begin{bmatrix} a \\ b \\ c \\ d \end{bmatrix}$$

and,

Equation 14

$$\dot{q} = \begin{bmatrix} \dot{a} \\ \dot{b} \\ \dot{c} \\ \dot{d} \end{bmatrix} = \frac{1}{2}\begin{bmatrix} a & -b & -c & -d \\ b & a & -d & c \\ c & d & a & -b \\ d & -c & b & a \end{bmatrix} * \begin{bmatrix} 0 \\ R_x \\ R_y \\ R_z \end{bmatrix}$$

where,

- a, b, c, d are quaternion parameters,
- R_x, R_y, R_z are the final angular velocity information of each axis from *Equation 6*.

That is, from the gyroscope's measurements, the user can solve the quaternion differential *Equation 14* to get the updated quaternion, and then use the following equation to get the updated DCM which leads to updated Euler angles from *Equation 12*.

Equation 15

$$C_b^n = \begin{bmatrix} (a^2 + b^2 - c^2 - d^2) & 2(bc - ad) & 2(bd + ac) \\ 2(bc + ad) & (a^2 - b^2 + c^2 - d^2) & 2(cd - ab) \\ 2(bd - ac) & 2(cd + ab) & (a^2 - b^2 - c^2 + d^2) \end{bmatrix}$$

7 References

1. Webseminar: "MEMS gyroscopes: their main applications, internal structure, working principles"
2. L3G4200D datasheet
3. Linear accelerometers in LGA package surface mounting guidelines (TN0018)
4. D.H. Titterton, "Strapdown Inertial Navigation Technology" 2nd Edition, The institute of Electrical Engineers, 2004.

8 Revision history

Table 2. Document revision history

Date	Revision	Changes
25-Jul-2011	1	Initial release.

Please Read Carefully:

Information in this document is provided solely in connection with ST products. STMicroelectronics NV and its subsidiaries (“ST”) reserve the right to make changes, corrections, modifications or improvements, to this document, and the products and services described herein at any time, without notice.

All ST products are sold pursuant to ST’s terms and conditions of sale.

Purchasers are solely responsible for the choice, selection and use of the ST products and services described herein, and ST assumes no liability whatsoever relating to the choice, selection or use of the ST products and services described herein.

No license, express or implied, by estoppel or otherwise, to any intellectual property rights is granted under this document. If any part of this document refers to any third party products or services it shall not be deemed a license grant by ST for the use of such third party products or services, or any intellectual property contained therein or considered as a warranty covering the use in any manner whatsoever of such third party products or services or any intellectual property contained therein.

UNLESS OTHERWISE SET FORTH IN ST’S TERMS AND CONDITIONS OF SALE ST DISCLAIMS ANY EXPRESS OR IMPLIED WARRANTY WITH RESPECT TO THE USE AND/OR SALE OF ST PRODUCTS INCLUDING WITHOUT LIMITATION IMPLIED WARRANTIES OF MERCHANTABILITY, FITNESS FOR A PARTICULAR PURPOSE (AND THEIR EQUIVALENTS UNDER THE LAWS OF ANY JURISDICTION), OR INFRINGEMENT OF ANY PATENT, COPYRIGHT OR OTHER INTELLECTUAL PROPERTY RIGHT.

UNLESS EXPRESSLY APPROVED IN WRITING BY TWO AUTHORIZED ST REPRESENTATIVES, ST PRODUCTS ARE NOT RECOMMENDED, AUTHORIZED OR WARRANTED FOR USE IN MILITARY, AIR CRAFT, SPACE, LIFE SAVING, OR LIFE SUSTAINING APPLICATIONS, NOR IN PRODUCTS OR SYSTEMS WHERE FAILURE OR MALFUNCTION MAY RESULT IN PERSONAL INJURY, DEATH, OR SEVERE PROPERTY OR ENVIRONMENTAL DAMAGE. ST PRODUCTS WHICH ARE NOT SPECIFIED AS "AUTOMOTIVE GRADE" MAY ONLY BE USED IN AUTOMOTIVE APPLICATIONS AT USER’S OWN RISK.

Resale of ST products with provisions different from the statements and/or technical features set forth in this document shall immediately void any warranty granted by ST for the ST product or service described herein and shall not create or extend in any manner whatsoever, any liability of ST.

ST and the ST logo are trademarks or registered trademarks of ST in various countries.

Information in this document supersedes and replaces all information previously supplied.

The ST logo is a registered trademark of STMicroelectronics. All other names are the property of their respective owners.

STMicroelectronics group of companies

Australia - Belgium - Brazil - Canada - China - Czech Republic - Finland - France - Germany - Hong Kong - India - Israel - Italy - Japan - Malaysia - Malta - Morocco - Philippines - Singapore - Spain - Sweden - Switzerland - United Kingdom - United States of America

www.st.com